JOINT INSTITUTE FOR NUCLEAR RESEARCH
Flerov Laboratory of Nuclear Reactions

September 27 - November 05 2021, Wave 5
Final report of the INTEREST programme

Determination of masses of the super heavy elements in the experiments on synthesis of Cn and Fl using the reactions ^{48}Ca + ^{242}Pu and ^{48}Ca + ^{244}Pu

Student

Jakub Sochor
Czech Technical University in Prague,
Faculty of Nuclear Sciences and Physical
Engineering, Department of Nuclear
Chemistry
ORCID 0000-0002-6637-9549
jakub.sochor@fjfi.cvut.cz

Supervisor

Viacheslav Vedeneev
Flerov Laboratory of Nuclear Reactions

Date and place

Prague, 2021

Abstract

The synthesis of superheavy elements (SHE) and research of their chemical properties is one of the main topics of current nuclear physics and chemistry. Unfortunately, the large energy requirements, small yields (in the order of atomic units), and sometimes even immeasurably small half-lives of the reactions performed so far do not allow to carry out all basic research on superheavy elements. Tests of new technologies and devices thus occur with homologues, which should have approximately the same chemical properties. This is also the case in these experiments, where mercury and radon are used for copernicium research in MASHA setup (Flerov Laboratory of Nuclear Reactions, Joint Institute for Nuclear Research in Dubna, Russia) on the basis of chemical similarity based on the periodic law.

Key words: Mass-separator · ECR ion source · Hot catcher · Separation efficiency · Superheavy elements · Copernicium · Flerovium

1 Introduction

Research and synthesis of superheavy elements (SHE) is one of the most important topics not only in the second half of the 20th century but also in today's nuclear physics and chemistry. Due to the short half-lives of these very heavy nuclei, great demands are placed on the use of synthesis and analytical equipment. Accelerators must be able to generate considerable energy, analytical equipment must be able to analyze in the order of seconds and only units of atoms. For these reasons, lighter homologues of superheavy elements, which have similar properties due to the periodic law, are used in testing the new apparatus. Research into these superheavy elements is motivated not only by the presumed unusual chemical and physical properties, but also by the discovery of an island of stability, where the elements should be stable despite their large weight

This method of experimental work was also used for experiments with MASHA apparatus at the Flerov Laboratory of Nuclear Reactions, part of Joint Institute for Nuclear Research in Dubna, Russia, whose part is described in this report.

Project goals

To perform the mass measurement and determination of short-lived isotopes of Hg (as the homologue to SHE), Rn and its daughter nuclei by α-decay chains using a position sensitive Si detector. Simultaneous yield measurements of Cn, Fl, and Hg.

2 Theoretical part

2.1 Joint Institute for Nuclear Research

Joint Institute for Nuclear Research (JINR), founded in 1956, is a scientific institution based in Dubna, Russia, near Moscow. The work is based on the international cooperation of 18 countries. At present, it is one of the world's leading workplaces in the field of nuclear physics and chemistry, not only thanks to top scientific staff, but also equipment including (among others) particle accelerators, cyclotrons, phasotron and synchrophasotron. [2]

Flerov Laboratory of Nuclear Reactions (FLNR), founded in 1957, is one of the eight departments of JINR. Research work in this department is known worldwide mainly due to the synthesis of new superheavy elements (and new isotopes of SHE), which in four cases received names in honor of this research facility: dubnium (Z = 105, named after the city Dubna), flerovium (Z = 114, named in honor of the Soviet nuclear physicist Georgy Flyorov), moscovium (Z = 115, named after the Moscow region) and oganesson (Z = 118, named in honor of Russian nuclear physicist Yuri Oganessian). [2]

2.2 Copernicium

Copernicium (Z = 112) is one of the two elements whose production has been investigated in this work. Cn is the heaviest member of the 12th group of the periodic table (this group is consists of zinc, cadmium, and mercury) with electron configuration [Rn] $5f^{14}$ $6d^{10}$ $7s^2$. However, due to the relativistic effects in the field of such heavy elements and lanthanide contraction, a purely theoretical prediction of the properties is almost impossible. Experiments and associated calculations indicate that copernicium should be (at room temperature) an unstable liquid (melting point 283 ± 11 K) with a density similar to mercury. Considerable inertness of the element is also assumed, which led to the designation of copernicium as a noble metal. [4]

In 2021 there are 13 known isotopes of copernicium, 5 of them have known half-lifes. The most stable isotope is ^{285}Cn with $T_{1/2} = 30$ s which is enough to examine its chemical properties. [5]

2.3 Flerovium

Flerovium (Z = 114) is the second of the studied elements with electron configuration [Rn] $5f^14$ $6d^{10}$ $7s^2$ $7p^2$. Due to the relativistic effects and stabilization of $7s^2$ orbitals, as with Cn, there is a presumption of lower chemical reactivity than with its lighter homologues. [9]

Flevorium (aka eka-plubum or element 114) was discovered by the Dubna-Livermore collaboration in 2000 and IUPAC approved its name in 2012. [9] In 2021 there are 8 known isotopes of flerovium, 6 of them have known half-lifes. The most stable isotope is ^{289}Fl with $T_{1/2} = 2,7$ s. [5]

2.4 MASHA setup

The basis of the experimental apparatus was a device called MASHA (***M**ass **A**nalyser of **S**uper **H**eavy **A**toms*). Its current layout (after many modifications and modernizations in recent years [3]) for this experimental campaign is at Figure 1.
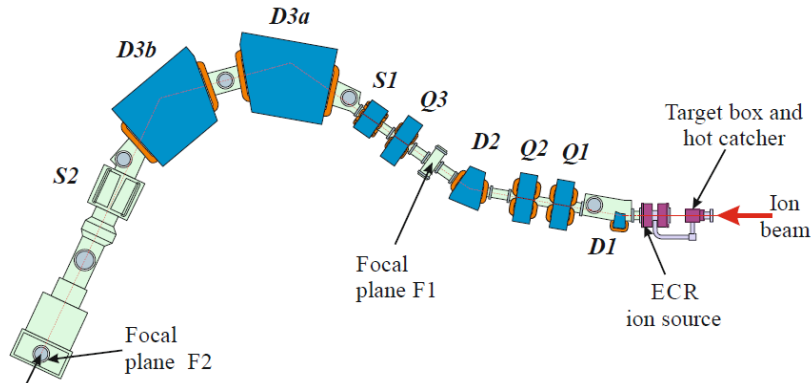
Figure 1: Scheme of the MASHA setup [6] *(description of individual parts in the text)*

Ion beam comes from U-400M cyclotron with 5 mm beam input diameter. [1]

Target box and hot catcher contains a rotating target (the rotation of the target was designed for uniform heating and thus less thermal effect on the reactions and better efficiency), wherein the frequency of rotation of the target by the electric motor by Siemens is 25 Hz. Hot catcher, 0.6 mm thick and 30 mm diameter disk made of flexible graphite, is heated to 1800-2000°C. [8]

ECR ion source A microwave oscillator with a frequency of ultra-high frequency 2.45 GHz is used to ionize the atoms (with an efficiency of up to 90 % in certain cases) formed by the nuclear reaction with charge state +1, [7] at the same time it accelerates ions to energies up to 38 keV. The walls of the source, as well as all other pipes and detectors, are covered with a layer of titanium nitride TiN (with chemical properties partially similar to ceramics) to prevent any chemical reactions of ions with the environment. Helium serves here as a buffer gas at a total pressure of about $(1-2) \cdot 10^{-3}$ Pa. [8]

D1, D2, D3a and D3b are dipole magnets. [7]

Q1, Q2 and Q3 are quadruple lenses. [7]

S1 and S2 are sextupole lenses. [7]

F1 and F2 are focal planes. In the second focal plane, there is a detection system (with 1,25 mm pitch). The main part of it is the special 192 front strip silicon detector in which there is a vacuum. In this case, the measurement geometry (described in detail in the source [7]) guarantees the capture of more than 90 % of the alpha

particles emitted by the resulting atoms, which, due to their weight, will be in the vast majority the alpha emitters. All signals (with information about energy and strip number) caused by the capture of alpha particles are immediately transmitted to the counter. The detectors are calibrated directly on alpha particles with an energy of up to 20 MeV (other detectors are designed for fission products that have a higher energy and the calibration is therefore up to 200 MeV). [7]

3 Methods

Evaluation of all obtained data was performed in the Origin program (OriginLab Corporation) version 2020b according to the working methodology provided by the project supervisor. In general, the nuclear reactions described below result in strongly excited nuclei that emit their excess energy by neutron ejection (up to eight). It follows that the obtained nuclei will be significantly neutrodeficient and, due to their weight, alpha transformation or electron capture will be observed. The half-lives will also be significantly short, in the order of a maximum of tens of seconds, which is close to the half-lives of the nuclides of superheavy elements described so far.

3.1 Expected nuclear reactions

Half-life and types of radioactive transformations are from the source [5].

Argon-40 beam and samarium-148 target:

$$^{148}_{62}\text{Sm}(^{40}_{18}\text{Ar}; 3\text{n})^{185}_{80}\text{Hg} \tag{1a}$$

$$^{148}_{62}\text{Sm}(^{40}_{18}\text{Ar}; 4\text{n})^{184}_{80}\text{Hg} \tag{1b}$$

$$^{148}_{62}\text{Sm}(^{40}_{18}\text{Ar}; 5\text{n})^{183}_{80}\text{Hg} \tag{1c}$$

$$^{148}_{62}\text{Sm}(^{40}_{18}\text{Ar}; 6\text{n})^{182}_{80}\text{Hg} \tag{1d}$$

$$^{148}_{62}\text{Sm}(^{40}_{18}\text{Ar}; 7\text{n})^{181}_{80}\text{Hg} \tag{1e}$$

$$^{148}_{62}\text{Sm}(^{40}_{18}\text{Ar}; 8\text{n})^{180}_{80}\text{Hg} \tag{1f}$$
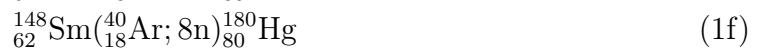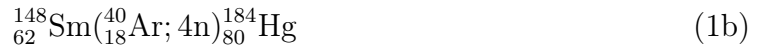
$^{185}_{80}\text{Hg}$ (as a reaction product 1a): 94 % ε, 6 % α, $T_{\frac{1}{2}} = 49.1$ s

$^{184}_{80}\text{Hg}$ (as a reaction product 1b): 98.89 % ε, 1.11 % α, $T_{\frac{1}{2}} = 30.87$ s

$^{183}_{80}\text{Hg}$ (as a reaction product 1c): 88.3 % ε, 11.7 % α, $2.6 \cdot 10^{-4}$ % ε p, $T_{\frac{1}{2}} = 9.4$ s

$^{182}_{80}\text{Hg}$ (as a reaction product 1d): 86.2 % ε, 13.8 % α, $T_{\frac{1}{2}} = 10.83$ s

$^{181}_{80}\text{Hg}$ (as a reaction product 1e): 73 % ε, 27 % α, $2.6 \cdot 0.01$ % ε p, $T_{\frac{1}{2}} = 3.6$ s

$^{180}_{80}\text{Hg}$ (as a reaction product 1f): 52 % ε, 48 % α, $T_{\frac{1}{2}} = 2.59$ s

Argon-40 beam and erbium-166 target:

$$^{166}_{68}\text{Er}(^{40}_{18}\text{Ar}; 1n)^{205}_{86}\text{Rn} \tag{2a}$$

$$^{166}_{68}\text{Er}(^{40}_{18}\text{Ar}; 2n)^{204}_{86}\text{Rn} \tag{2b}$$

$$^{166}_{68}\text{Er}(^{40}_{18}\text{Ar}; 3n)^{203}_{86}\text{Rn} \tag{2c}$$

$$^{166}_{68}\text{Er}(^{40}_{18}\text{Ar}; 4n)^{202}_{86}\text{Rn} \tag{2d}$$

$$^{166}_{68}\text{Er}(^{40}_{18}\text{Ar}; 5n)^{201}_{86}\text{Rn} \tag{2e}$$

$^{205}_{86}\text{Rn}$ (as a reaction product 2a): 75.4 % ε, 24.6 % α, $T_{\frac{1}{2}} = 170$ s

$^{204}_{86}\text{Rn}$ (as a reaction product 2b): 72.4 % α, 27.6 % ε, $T_{\frac{1}{2}} = 74.5$ s

$^{203}_{86}\text{Rn}$ (as a reaction product 2c): 66 % α, 34 % ε, $T_{\frac{1}{2}} = 44$ s

$^{202}_{86}\text{Rn}$ (as a reaction product 2d): 78 % α, 22 % ε, $T_{\frac{1}{2}} = 9.7$ s

$^{201}_{86}\text{Rn}$ (as a reaction product 2e): ? α, ? ε, $T_{\frac{1}{2}} = 7$ s

Calcium-48 beam and plutonium-242 target:

Due to the high excitation energies of such compound nuclei formed by reactions, de-excitation is not only possible by neutron emission, but by larger nuclei that are not directly identifiable. Only the resulting products can be identified.

$$^{242}_{94}\text{Pu}(^{48}_{20}\text{Ca}; \text{multi-nucleon transfer})^{219}_{86}\text{Rn} \tag{3a}$$

$$^{242}_{94}\text{Pu}(^{48}_{20}\text{Ca}; \text{multi-nucleon transfer})^{218}_{86}\text{Rn} \tag{3b}$$

$$^{242}_{94}\text{Pu}(^{48}_{20}\text{Ca}; \text{multi-nucleon transfer})^{212}_{86}\text{Rn} \tag{3c}$$

$^{219}_{86}\text{Rn}$ (as a reaction product 3a): 100 % α, $T_{\frac{1}{2}} = 3.96$ s

$^{218}_{86}\text{Rn}$ (as a reaction product 3b): 100 % α, $T_{\frac{1}{2}} = 35$ ms

$^{212}_{86}\text{Rn}$ (as a reaction product 3c): 100 % α, $T_{\frac{1}{2}} = 0.54$ ms

4 Results

Due to the energies used in the measurement, all captured peaks in this chapter are caused by the alpha transformation of the radioactive nuclei. In original data there are also negative Y definitions (counts below zero). The reason is that some strange signals are coming from multiplexers and algorithm of electronics reduces it wrongly.

4.1 Argon-40 beam and samarium-148 target
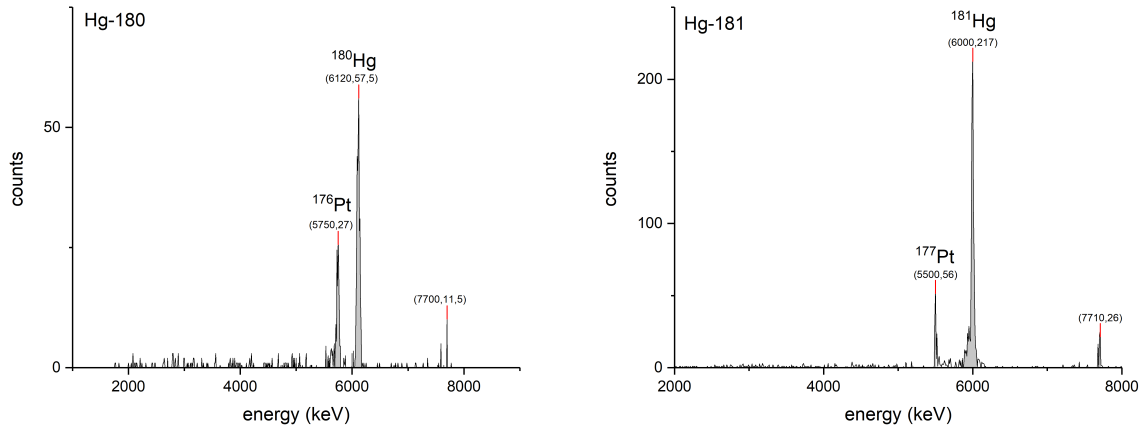
(a) Spectrum for Hg-180

(b) Spectrum for Hg-181

Figure 2: Spectres for Hg-180 and Hg-181

Spectrum on figure 2a is experimentally measured spectrum for **Hg-180** which is produced as described in equation 1f. There is a peak at energy 6120 keV which is a peak of Hg-180 with intensity of 47.9 %. Its daughter, Pt-176 (Hg-180 has 48 % probability of alpha decay), has the visible peak at energy 5750 keV with intensity 40 %. The other 52 % of decay probability is electron capture which comes to Au-180 whose decay (peaks) is not good known (98 % of Au-180 decays to Pt-180 which peak 5140 keV cannot be seen in spectrum because of low intensity 0.28 %). Furthermore, any other daughters of Pt-176 (Ir-176, Os-172, Os-176) are not recognizable in the spectrum.

Peak with energy 7700 keV unfortunately cannot be identified. Due to the fact that this peak is more or less visible on all spectra, it is probably some background nuclide or pollution from previous experimental campaigns.

Spectrum 2b is experimentally measured spectrum for **Hg-181** which is produced as described in equation 1e. There is a peak at energy 6000 keV which is a peak of Hg-181 with intensity of 21.4 %. Its daughter, Pt-177 (Hg-181 has 27 % probability of alpha decay), has the visible peak at energy 5500 keV.

(a) Spectrum for Hg-182

(b) Spectrum for Hg-183
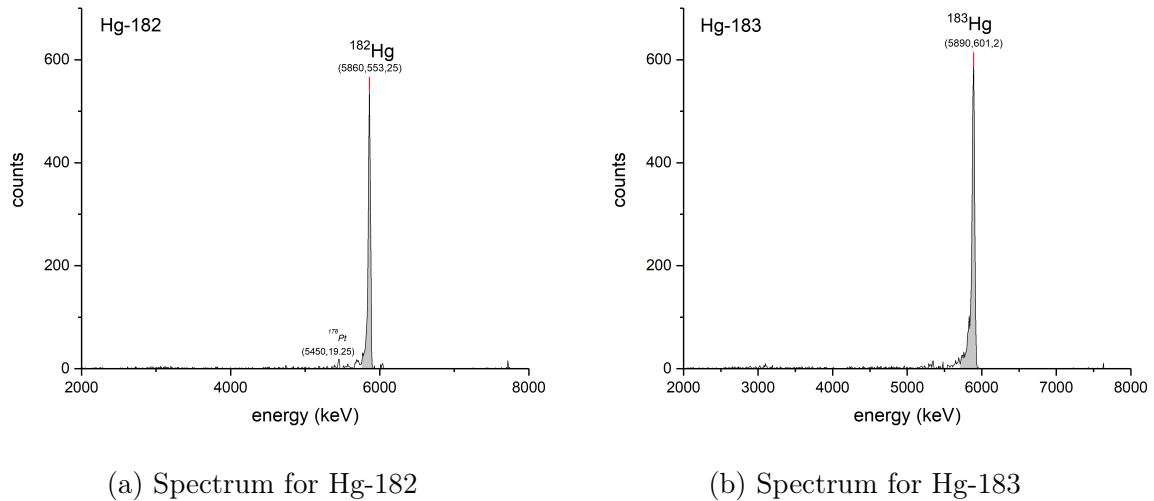
Figure 3: Spectres for Hg-182 and Hg-183

Spectrum on figure 3a is experimentally measured spectrum for **Hg-182** which is produced as described in equation 1d. There is a peak at energy 5860 keV which is a peak of Hg-182 with intensity 15 %. It has 86 % probability to electron capture and 14 % to alpha decay. Daughter of Hg-182 electron capture is Au-182 whose peaks have a minimal intensity (about 0.1 %) and cannot be seen in spectres. The product of Hg-182 alpha decay is Pt-178 with an important peak at energy 5450 keV with intensity 4 % which is on the Figure 3a next to big peak. Peak at energy about 7700 keV is also easily recognizable but cannot be identified (see above).

Spectrum on figure 3b is experimentally measured spectrum for **Hg-183** which is produced as described in equation 1c. The main peak for this nuclide is at energy 5890 keV with intensity 11 % which come from alpha decay. Peak 5195 keV (with intensity 0.24 %) which belongs to the daughter Pt-179, was not measured. Likewise, no other daughters or their peaks were observed. Peak with energy about 7700 keV is also easily recognizable but cannot be identified (see above).

Spectrum on figure 4a is experimentally measured spectrum for **Hg-184** which is produced as described in equation 1b. The main peak for this nuclide is at energy 5530 keV with intensity 1.25 % which come from alpha decay. Other peaks of this nuclide have an intensity about 0.005 % which is too low to observe. Unfortunately, the peak at energy 6030 keV cannot be identified - the vast majority of daughters are transformed exclusively by electron capture, and the intensities of individual peaks of partial alpha transformation are not sufficiently represented to form such a large peak. Thus, the sample may have been contaminated, or other unexpected radionuclides may have formed.

Spectrum on figure 4b is experimentally measured spectrum for **Hg-185** which is pro-

duced as described in equation 1a. The main peak for this nuclide is at energy 5650 keV with intensity 5.8 % which come from alpha decay. The other recognised peak is at energy 5080 keV (intensity 0.26 %) which belongs to Au-185. This radionuclide is made through electron capture from Hg-185. No other peaks were visible in the spectrum.

(a) Spectrum for Hg-184

(b) Spectrum for Hg-185
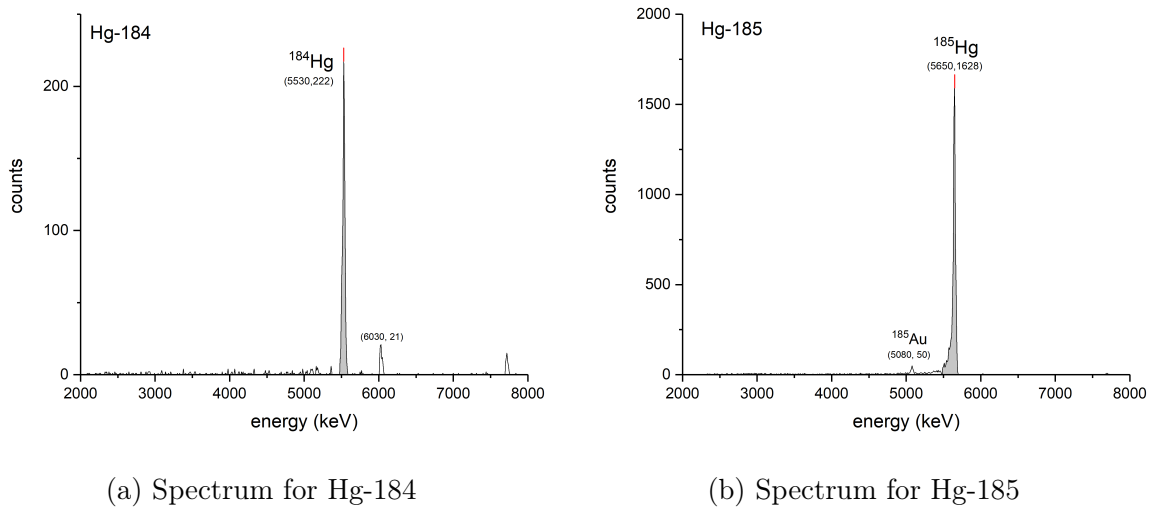
Figure 4: Spectres for Hg-184 and Hg-185

Heatmap on figure 5 symbolizes the counts of gained mercury radionuclides depending on the energy (the energy values had to be calibrated before plotting on the heatmap, according to the instructions from the supervisor).
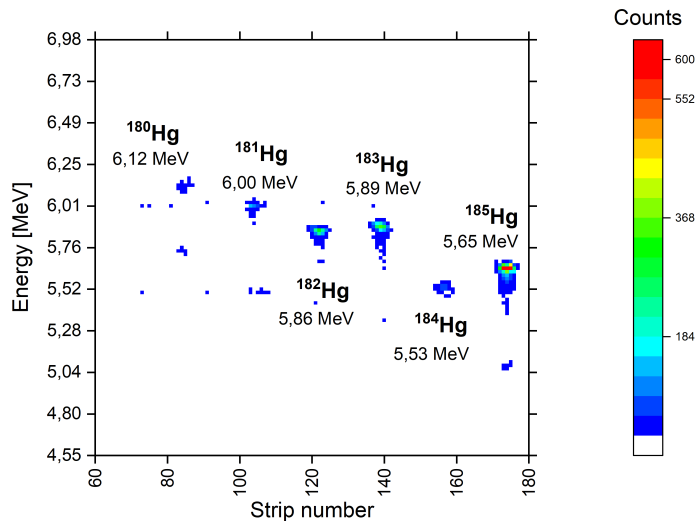
Figure 5: Heatmap for mercury radioisotopes

4.2 Argon-40 beam and erbium-166 target
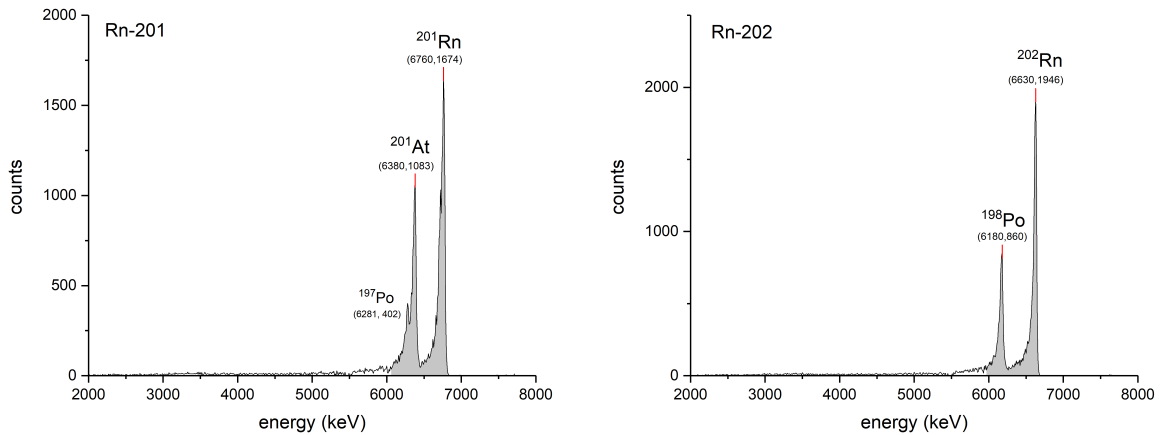
(a) Spectrum for Rn-201   (b) Spectrum for Rn-202

Figure 6: Spectres for Rn-201 a Rn-202

Spectrum on figure 6a is experimentally measured spectrum for **Rn-201** which is produced as described in equation 2e. The highest peak (with 1674 counts) belongs to Rn-201 with intensity 90 %. The other big peak probably comes from its daughter - At-201 which is made through electron capture. The tabulated value of this peak is 6342 keV, and this peak in the spectrum has 6380 keV. Due to the high intensity of the astatine peak, the high counts of the peak in the spectrum, and the relatively high probability of the formation of this nuclide, this difference in energy was neglected and the given peak was assigned to the astatine. The parasitic peak on the left side of the At-201 peak (with an energy of 6281 keV) was identified as the Po-197 peak (with an intensity of 59 %). This radionuclide Po-197 is the daughter of At-201 transformed by alpha conversion. An unidentified peak with an energy of approximately 7700 keV, which was noticeable on the previous spectra, now only turns into noise.

Spectrum on figure 6b is experimentally measured spectrum for **Rn-202** which is produced as described in equation 2d. The main peak at energy 6630 keV belongs to Rn-202 which has intensity about 78 %. The another peak (at energy 6180 keV and intensity 58 %) is peak of Rn-202's alpha daughter - Po-198. No further peaks were detected in the spectrum.

Spectrum on figure 7a is experimentally measured spectrum for **Rn-203** which has a peak with energy 6550 keV and which is produced as described in equation 2c. It has 608 counts and intensity 75 %. The alpha daughter of Rn-203 is the metastable Po-199m, which has a peak next to it at energy 6060 keV with intensity 39 %. the ground state of this radionuclide is then also visible in the spectrum, in the form of a slightly overlooked

peak at an energy of 5960 keV with intensity 12 %. Any additional peaks of other radon radionuclide daughters are indistinguishable from detector and background noise.

(a) Spectrum for Rn-203   (b) Spectrum for Rn-204
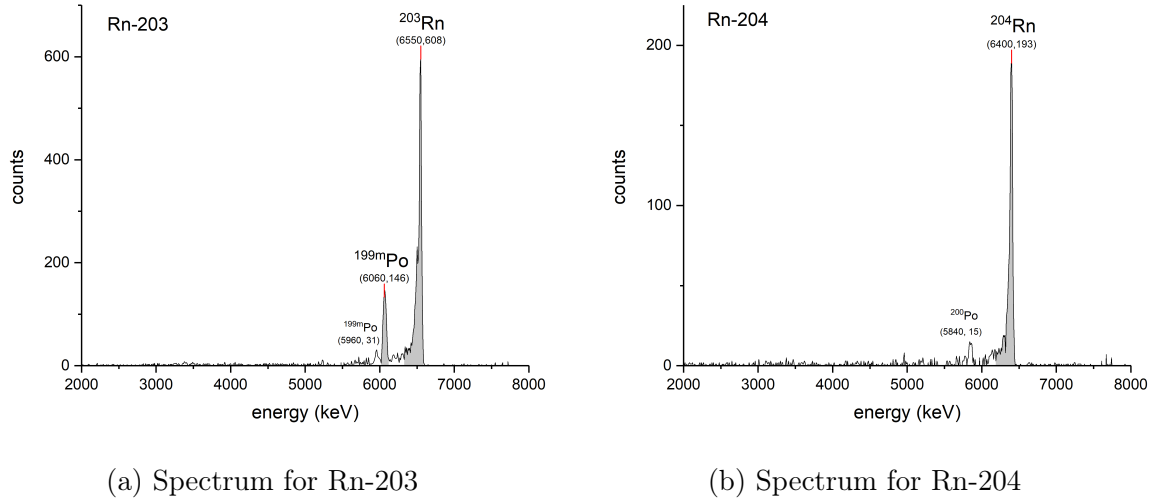
Figure 7: Spectres for Rn-203 and Rn-204

Spectrum on figure 7b is experimentally measured spectrum for **Rn-204** which is produced as described in equation 2b. The dominant peak in this spectrum is the peak at an energy of 6400 keV, which can be assigned to the radionuclide Rn-204. The tabulated value of this peak is 18 keV higher, but due to the high intensity (100 %) there is a high probability of misidentification. The second identified peak is the peak at an energy of 5840 keV, which belongs to the alpha daughter Rn-204, namely, the Po-200 with an intensity of 11 %. Due to the fact that even in this case the tabulated peak value is about 21 keV higher, there is a probability of incorrect calibration of the detector. Peak at an energy value of about 7700 keV is again visible on this spectrum, but unfortunately it is still unidentifiable.

Spectrum on figure 8 is experimentally measured spectrum for **Rn-205** (which is produced as described in equation 2a) and it is the last spectrum for the argon-40 beam and erbium-166 target. It must be taken into account that the counts are an order of magnitude lower compared to the previous spectra, and in this case the effect of the background noise will be significantly more pronounced. Despite this difficulty, however, two peaks can be identified - the basic peak Rn-205 with an energy of 6270 keV (and intensity 24.2 %) and the peak of its daughter (created by electron capture) At-205 at an energy of 5910 keV (intensity 10 %).
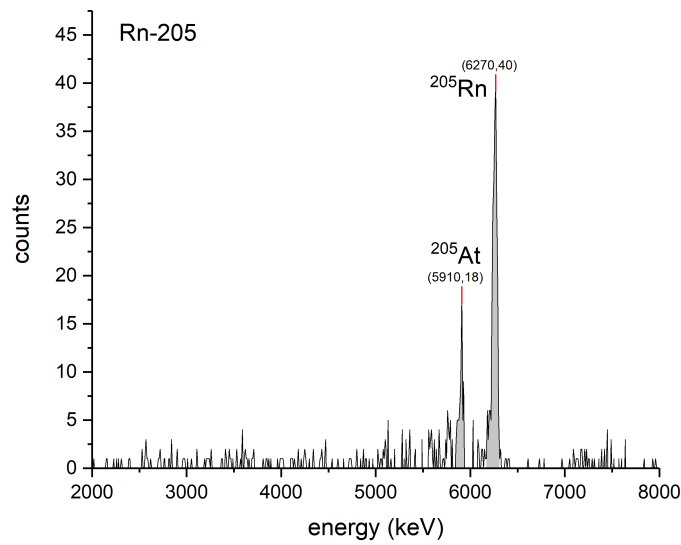
Figure 8: Spectrum for Rn-205

Heatmap on figure 9 symbolizes the counts of gained mercury radionuclides depending on the energy (the energy values had to be calibrated before plotting on the heatmap, according to the instructions from the supervisor).
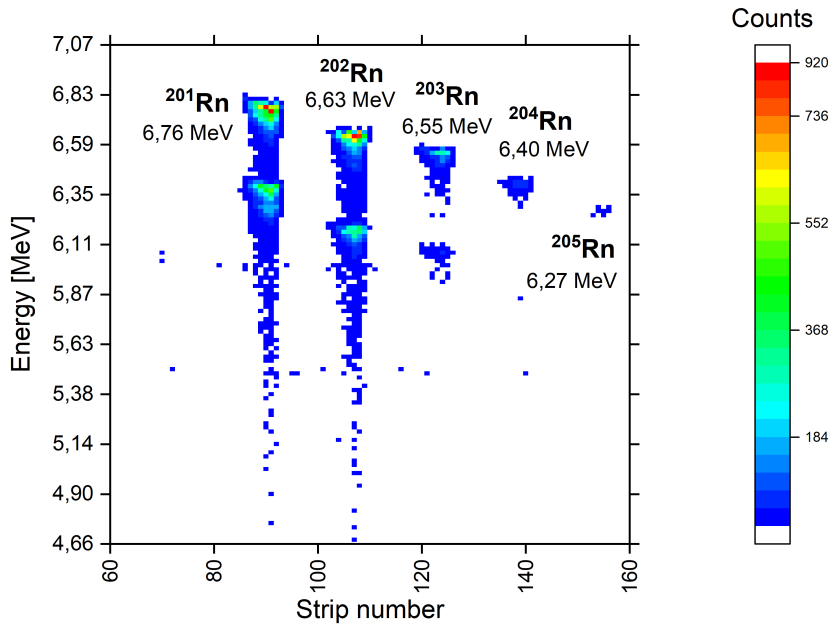
Figure 9: Heatmap for radon radioisotopes

4.3 Calcium-48 beam and plutonium-242 target
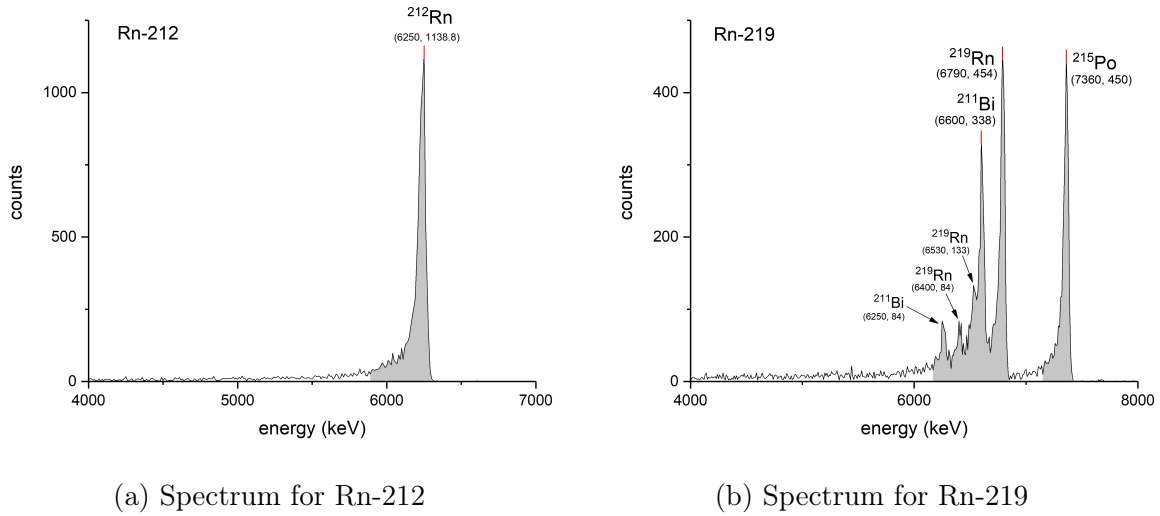
(a) Spectrum for Rn-212

(b) Spectrum for Rn-219

Figure 10: Spectres for Rn-212 a Rn-219

Spectrum on figure 10a is experimentally measured spectrum for **Rn-212** which is produced as described in equation 3c. This spectrum has significantly higher counts than the spectra obtained for other radionuclides in this experimental campaign (see figures 10b and 11). For this reason, the identification of peaks is much clearer. In this case, only one peak belonging to Rn-212 was identified (energy 6250 keV, 1139 counts, intensity 99.95 %). The alpha daughter of the radionuclide Rn-212 is Po-208 with a major peak around 5115 keV. However, it is not visible on the spectrum, due to the large half-life, which is almost 3 years, and during a short measurement, a sufficient number of counts is not recorded.

Spectrum on figure 10b is experimentally measured spectrum for **Rn-219** which is produced as described in equation 3a. A large number of peaks and radionuclides were identified in this spectrum (despite relatively low counts). The main peak Rn-219 was found to be 6790 keV (with an intensity of 79.4 %; tabulated value 6819 keV). Secondary, less visible but identifiable peaks of the same radionuclide are the peaks at 6400 keV (intensity 7.5 %, tabulated value 6425 keV) and 6530 keV (intensity 12.9 %, tabulated value 6553 keV, parasitic at the peak with energy 6600 keV).

The alpha daughter of the radionuclide Rn-219 is the radionuclide Po-215, which is visible at the peak with an energy of 7360 keV (intensity almost 100 %, tabulated energy 7386 keV). The third radionuclide identified is Bi-211, which was identified by a main energy peak of 6600 keV (intensity 83.54 %, tabulated value 6623 keV) and a secondary energy peak of 6250 keV (intensity 16.19 %, tabulated value 6278 keV). However, the mechanism of formation of this radionuclide is not the alpha of Po-215, as it might seem,

but in a more complicated, but realistic way:
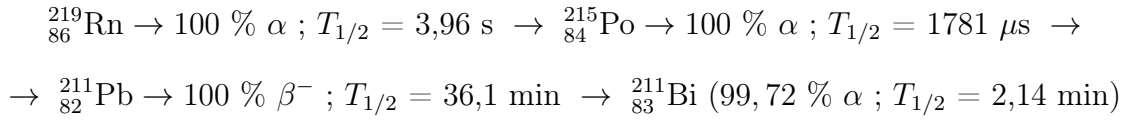
$$^{219}_{86}\text{Rn} \rightarrow 100 \text{ \% } \alpha \text{ ; } T_{1/2} = 3{,}96 \text{ s } \rightarrow \text{ } ^{215}_{84}\text{Po} \rightarrow 100 \text{ \% } \alpha \text{ ; } T_{1/2} = 1781 \text{ } \mu\text{s } \rightarrow$$

$$\rightarrow \text{ } ^{211}_{82}\text{Pb} \rightarrow 100 \text{ \% } \beta^- \text{ ; } T_{1/2} = 36{,}1 \text{ min } \rightarrow \text{ } ^{211}_{83}\text{Bi } (99{,}72 \text{ \% } \alpha \text{ ; } T_{1/2} = 2{,}14 \text{ min})$$

There is also the possibility of contamination of the spectrum by naturally occurring radionuclides, as the resulting Rn-219, Po-215, Pb-211, and Bi-211 are part of a naturally occurring actinium decay series. Due to more or less the same deviations of the experimental from the tabulated energy values, it is reasonable to consider a poor calibration of the detector, which should be solved in further experiments.
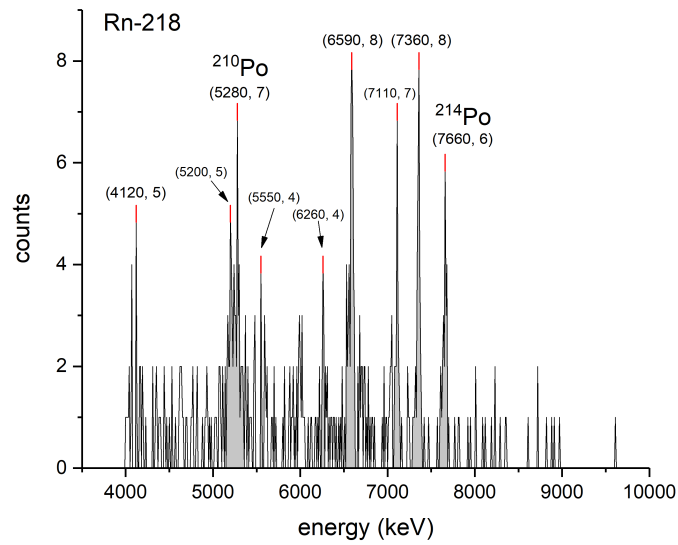
Figure 11: Spectrum for Rn-218

Spectrum on figure 11 is experimentally measured spectrum for **Rn-218** which is produced as described in equation 3b. Unfortunately, due to the really low activities, which are only in the order of units of counts, the search and identification of peaks were very difficult and there is a great possibility for errors. There is also the possibility of contamination of the spectrum by naturally occurring radionuclides, as the resulting polonium Po-214 is part of a naturally occurring uranium radium decay series.

Despite this fact, two of the peaks were identified. First peak with an energy of 7666 keV, which was assigned to the radionuclide Po-214 (intensity almost 100 %, tabulated energy 7687 keV). This radionuclide is the direct alpha daughter of Rn-218. The second peak is at energy 5287 keV and it was identified as Po-210 (intensity 100 %; tabulated energy 5304 keV). The mechanism of formation of this radionuclide is more complex

(and may not be correct), but it can be, from my point of view, realistic:

$$^{218}_{86}\text{Rn} \rightarrow 100 \ \% \ \alpha \ ; \ T_{1/2} = 35 \text{ ms} \rightarrow \ \ ^{214}_{84}\text{Po} \rightarrow 100 \ \% \ \alpha \ ; \ T_{1/2} = 164 \ \mu\text{s} \ \rightarrow$$

$$\rightarrow \ ^{210}_{82}\text{Pb} \rightarrow \ 100 \ \% \ \beta^- \ ; \ T_{1/2} = 22{,}2 \text{ y} \rightarrow \ ^{210}_{83}\text{Bi} \rightarrow \ 100 \ \% \ \beta^- \ ; \ T_{1/2} = 5{,}012 \text{ d} \rightarrow$$

$$\rightarrow \ ^{210}_{84}\text{Po} \ (100 \ \% \ \alpha \ ; \ T_{1/2} = 138{,}376 \text{ d})$$
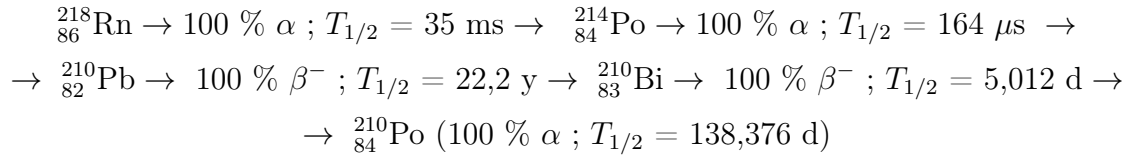
Other peaks were automatically detected by the Origin program in the spectrum, but it is very likely that they are random peaks caused by detector noise and background noise.
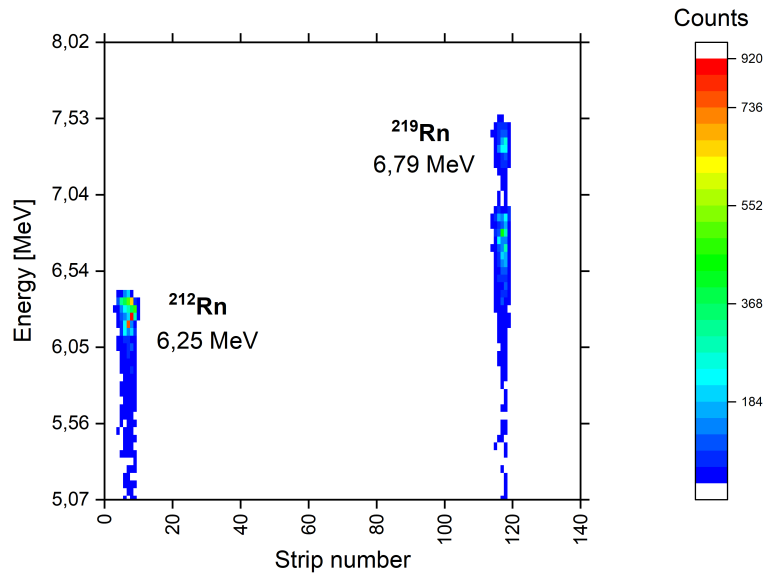
Figure 12: Heatmap for radon radioisotopes

Heatmap on figure 12 symbolizes the counts of gained mercury radionuclides depending on the energy (the energy values had to be calibrated before plotting on the heatmap, according to the instructions from the supervisor). The fact that even on this heatmap no trace of the radionuclide Rn-218 is visible only confirms the description of figure 11 that the peaks of the radionuclides obtained are not so visible that they can be unambiguously separated from the noise.

5 Conclusions

The functionality of the apparatus and detection device was proved, but it decreases with increasing mass number and decreasing half-life. However, this is also related to the parameters of the accelerator, when it is necessary to expend higher energy for higher

mass numbers and thus the assumption of a smaller number of cores. This increasing energy can also be seen in the presumed nuclear reactions, where compound nuclei need several neutrons ejected from lighter radionuclides for their deexcitation, while in the case of the hypothetical formation of flerovium, deexcitation is realized by ejection of larger nucleon units.

Therefore, the basis of the follow-up research should be a better balance of the projectile's energy so that a complex nucleus is formed, but only with such energy that deexcitation can occur only by neutron ejection, or other simple particles, and the superheavy element nucleus. However, from the point of view of chemical properties, no further problem should arise, since the synionuclides synthesized should be chemically similar to the radionuclides of superheavy elements.

Acknowledgements

References

[1] Abeer Attla, Lubos Krupa, and Aleksey Novoselov. *Experimental data analysis at the MASHA setup.* Dubna, 2016. URL: http://newuc.jinr.ru/img_sections/file/Practice2016/Egypt/ARE_Students%5C%20Presentations/11.%5C%20Abeer%5C%20Maher%5C%20Attia%5C%20Hassan.pdf.

[2] *Joint Institute for Nuclear Research. Science brings nations together.* Dubna, 2021. URL: http://www.jinr.ru/main-en/.

[3] Meruyert Mamatova et al. "Study of production stability of radon and mercury isotopes in complete fusion reactions at the mass-separator MASHA by "solid hot catcher" technique". In: *AIP Conference Proceedings* 2163.1 (2019), p. 070002. DOI: 10.1063/1.5130114. eprint: https://aip.scitation.org/doi/pdf/10.1063/1.5130114. URL: https://aip.scitation.org/doi/abs/10.1063/1.5130114.

[4] Jan-Michael Mewes et al. "Copernicium: A Relativistic Noble Liquid". In: *Angewandte Chemie International Edition* 58.50 (2019), pp. 17964–17968. DOI: https://doi.org/10.1002/anie.201906966. eprint: https://onlinelibrary.wiley.com/doi/pdf/10.1002/anie.201906966. URL: https://onlinelibrary.wiley.com/doi/abs/10.1002/anie.201906966.

[5] Brookhaven National Laboratory National Nuclear Data Center. *NuDat (Nuclear Structure and Decay Data).* Mar. 2008.

[6] A. Rodin et al. "Features of the Solid-State ISOL Method for Fusion Evaporation Reactions Induced by Heavy Ions". In: Jan. 2020, pp. 437–443. DOI: 10.1142/9789811209451_0062.

[7] A. Rodin et al. "MASHA separator on the heavy ion beam for determining masses and nuclear physical properties of isotopes of heavy and superheavy elements". In: *Instruments and Experimental Techniques* 57 (July 2014), pp. 386–393. DOI: 10.1134/S0020441214030208.

[8] V. Yu. Vedeneev et al. "The current status of the MASHA setup". In: *Hyperfine Interactions* 238.1 (2017). ISSN: 0304-3843. DOI: 10.1007/s10751-017-1395-9. URL: https://doi.org/10.1007/s10751-017-1395-9.

[9] Yakushev, Alexander and Eichler, Robert. "Gas-phase chemistry of element 114, flerovium". In: *EPJ Web Conf.* 131 (2016), p. 07003. DOI: 10.1051/epjconf/201613107003. URL: https://doi.org/10.1051/epjconf/201613107003.